

Predicting the Energy Demand of a Hardware Video Decoder with Unknown Design Using Software Profiling

Matthias Kränzler, Christian Herglotz, and André Kaup

Multimedia Communications and Signal Processing,

Friedrich-Alexander-Universität Erlangen-Nürnberg (FAU), Cauerstr. 7, 91058 Erlangen, Germany

Email: {matthias.kraenzler, christian.herglotz, and andre.kaup}@fau.de

Abstract—Energy efficiency for video communications and video-on-demand streaming is essential for mobile devices with a limited battery capacity. Therefore, hardware decoder implementations are commonly used to significantly reduce the energetic load of video playback. The energy consumption of such a hardware implementation largely depends on a previously published recommendation document of a video coding standard that specifies which coding tools and methods are included. However, during the standardization of a video coding standard, the energy demand of a hardware implementation is unknown. Hence, the hardware complexity of coding tools is judged subjectively by experts from the field of hardware programming without using standardized assessment procedures. This can lead to suboptimal decisions on rejection or acceptance of a coding tool. To solve this problem, we propose a method that accurately models the energy demand of existing hardware decoders with an average error of 1.79% by exploiting information from software decoder profiling. Motivated by the low estimation error, we propose a hardware decoding energy metric that can predict and estimate the complexity of an unknown hardware implementation using information from existing hardware decoder implementations and available software implementations of the future video decoder. By using multiple video coding standards for model training, we can predict the complexity of an unknown hardware decoder with a minimum error of 4.54% without using the corresponding hardware decoder for training.

Index Terms—Video Decoding, Hardware Complexity, Software Complexity, Energy, Modeling, Complexity Prediction

I. INTRODUCTION

MOBILE communications connect people worldwide over the Internet and are significant contributors to everyone’s entertainment. In recent years, it was observed that data traffic over mobile communications increased significantly. According to [1], the total mobile network traffic increased from 39.5 EB/month in 2019 to 154.7 EB/month in 2023. In 2028, the data traffic will reach 472 EB/month, corresponding to an increase of over ten times within nine years. This rise is mainly caused by the higher demand for video content, which contributed around 71% in 2023 and will increase to 80% by 2028.

Manuscript received July 02, 2024. Corresponding author: Matthias Kränzler. The authors are with the Chair of Multimedia Communications and Signal Processing, Friedrich-Alexander-Universität Erlangen-Nürnberg (FAU), Erlangen, Germany (e-mail: matthias.kraenzler@fau.de; andre.kaup@fau.de; christian.herglotz@fau.de).

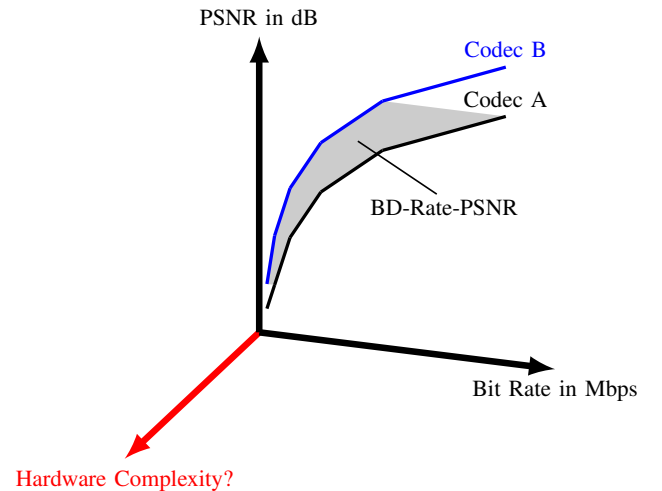


Fig. 1. In standardization, typically, the Bjøntegaard Delta Bit Rate PSNR (BDR-PSNR) metric is used to describe the bitrate savings of a newly proposed video coding specification (codec B) compared to a state-of-the-art video coding specification (codec A). Alternatively, the bit rate savings of a newly proposed coding tool compared to the anchor can be evaluated. The gray area between codec A and B corresponds to the bit rate savings that can be achieved with codec B. However, during standardization, the HW implementation complexity of codec B in terms of chip area and power demand is unknown and, therefore, can not be evaluated.

Simultaneously, according to [2], it is estimated that 1% of the global greenhouse gas emissions (GHG) were caused by video communications in 2018. Therefore, the rise in video communications also increases GHG emissions due to more watch time and data traffic. Consequently, it is crucial to improve the energy efficiency of video communications to reduce GHG emissions [3]. Furthermore, it is important to consider that the consumption of video content leads to a significant reduction in battery lifetime for mobile devices [4].

In order to address these challenges, the reduction of global video data traffic was targeted by standardization bodies such as ISO, ITU, or the Alliance for Open Media (AOM). AOM was founded in 2015 and finalized its first video coding standard AOMedia Video 1 (AV1) in 2018. The goal was an improved compression efficiency compared to state-of-the-art video coding standards such as High-Efficiency Video Coding (HEVC) or Advanced Video Coding (AVC). For ISO and ITU, the Joint Video Exploration Team (JVET) was founded in

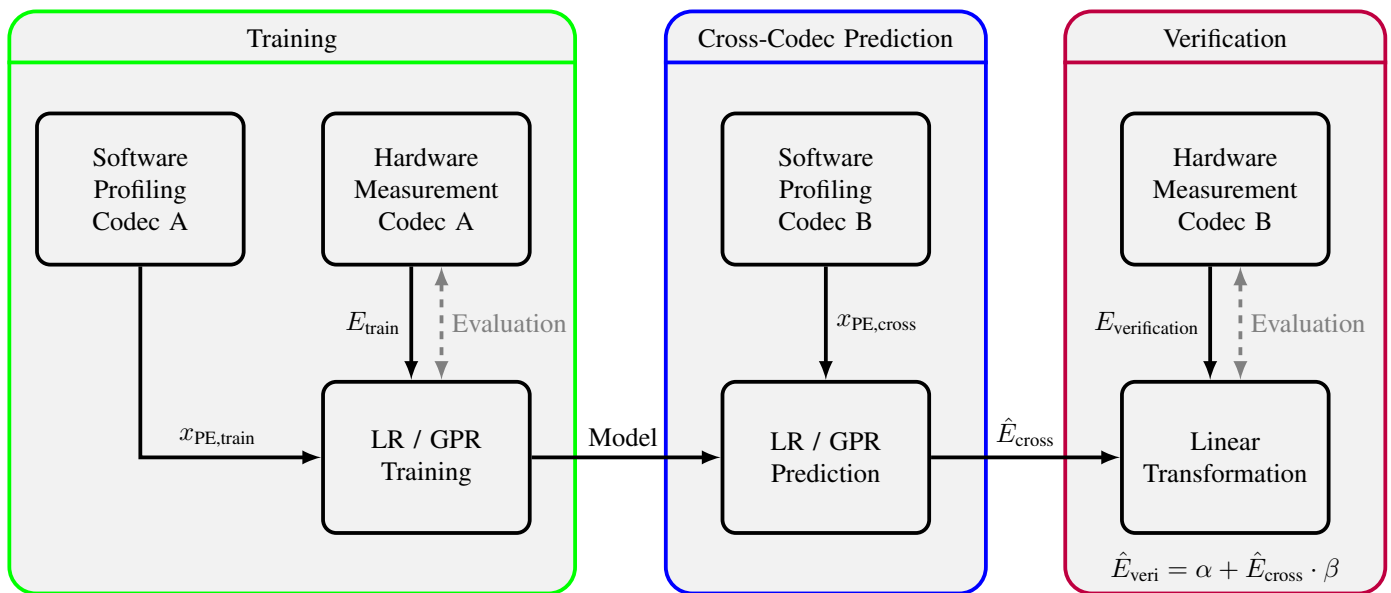


Fig. 2. Overview of the workflow for the developed metric and the evaluations that are presented in this paper. The workflow can generally be divided into the modules training, cross-codec prediction, and verification. We use a video coding standard with an available HW implementation for the training. This coding standard will be referred to as Codec A. For the cross-codec prediction, we use PEs from a software implementation of Codec B, which could be under development. We use a state-of-the-art video coding standard with an available HW implementation for verification to check the accuracy of the predictions.

2015 with the same goal. In 2020, the video coding standard Versatile Video Coding (VVC) was published. Even though both video coding standards improved compression efficiency, it was reported that the complexity of these video decoders increased significantly. According to [5], the energy demand of VVC is increased by over 80% in relation to HEVC for software (SW) decoding.

Figure 1 shows the problem that is faced during standardization of a new video coding standard. Usually, the standardization committee compares a state-of-the-art video coding standard (Codec A) with the newly proposed coding standard (Codec B). Then, the bit rate savings of codec B over codec A are evaluated in terms of Bjøntegaard Delta Bit Rate (BDR) [6], [7]. Typically, it is targeted to reduce the bit rate of a former coding standard by around 50%. However, the hardware (HW) complexity in terms of power demand and chip area cannot be evaluated during the standardization, because HW implementations are not yet available. Therefore, it is not possible to evaluate the HW complexity costs of newly proposed coding tools. Thus, tradeoffs between the compression efficiency and the energy efficiency cannot be evaluated. A worst-case scenario is a HW implementation with a high power demand that limits the support of high resolutions for mobile devices. This may also negatively affect the user's quality of experience due to a quickly draining battery.

In this work, we propose a method to predict the HW complexity measured by the energy demand of a future video coding standard using SW decoder implementations. These are typically available during the standardization process. Therefore, we will introduce our developed metric and methodology to provide a solution to predict the HW decoding energy demand using SW decoder profiling. To this end, this paper provides the following contributions:

- A HW decoder complexity evaluation in terms of energy demand.
- An evaluation framework using HW and SW implementations of decoders from six widely used video coding standards.
- A HW decoder energy model using SW decoder processor events (PEs).
- Gaussian process regression (GPR) to model and predict the energy demand of video decoding.
- Methodology to predict the HW decoder energy consumption of an unknown design.

An overview of the proposed methodology to predict the energy demand of an unknown HW video decoder implementation is shown in Figure 2. We use three modules to explain the methodology: training, cross-codec prediction, and verification. We use coding standards with an available SW and HW implementation for training, which we call Codec A. To train the energy models (green box in Figure 2), the energy demand of a given HW decoder is measured. Furthermore, the SW decoder implementations of Codec A are analyzed with instruction profilers such as Perf or Valgrind [8]. Thereby, we get the occurrences of the PEs such as instructions, memory accesses, branches, and cache misses (c.f., x_{PE}). The PEs are then used to train the corresponding energy models with linear regression (LR) or Gaussian process regression (GPR).

For the cross-codec prediction module (blue box in Figure 2), we utilize the pre-trained energy models from the training module in the context of another Codec B. We assume that we have no access to a HW implementation for codec B. Also, we want to provide an objective description of the hardware complexity. This scenario also applies to standardization, where an existing SW implementation is available. The SW profiling of this implementation can deliver the PEs that we

utilize for the cross-estimation of the energy demand \hat{E}_{cross} of the unknown HW implementation.

Finally, as indicated by the red box in Figure 2, we evaluate whether the developed energy models are accurate estimators in the context of cross-codec prediction of HW decoders' energy demand. Therefore, we use a coding standard with an available HW implementation that is different from the training coding standard. Then, we verify if the cross-codec prediction delivers meaningful energy estimates for the HW decoder of Codec B. We find that a linear transformation is required, because the cross-codec prediction is linearly scaled with the ground truth measurements of Codec B. This can be caused by the change of the technology node or the degree of HW optimization. In order to evaluate the cross-codec prediction, we linearly transform the prediction and compare it to the corresponding values of the actual HW measurement.

In this work, we will first present a literature review of previous work on analyzing, modeling, and optimizing video decoder complexity in Section II. After that, we introduce the evaluation setup and define our metrics utilized throughout the paper in Section III. Then, in Section IV, we will discuss the LR and GPR used to model the energy demand of the video decoders. Thereafter, the used energy models will be introduced. In Section V, the SW decoder energy demand is modeled by the energy models, which inspired us to model the HW energy demand using the SW complexity. In Section VI, we discuss how the energy demand of HW decoders can be modeled using SW decoders. Then, we will show in Section VII how an unknown video decoder HW design can be predicted with existing SW decoder implementations. Finally, we will conclude the paper in Section VIII with a summary of the findings and an outlook on future research.

II. LITERATURE REVIEW

In the literature, it is common to analyze the complexity of a video coding standards in terms of energy, time, and chip area first. Then, the observed experimental results can be modeled to understand the complexity and describe it by features derived through the analysis. Finally, those models can be utilized to optimize the corresponding complexity.

1) *Analysis*: The complexity of video coding was studied in multiple papers. In [9], the video coding standards HEVC, AVC, VVC, and AV1 were studied in terms of encoding time, decoding time, and compression efficiency. In [5], the energy demand of HEVC and VVC video decoders was studied, and optimization methods of the energy demand were also proposed. Other works studied VVC in relation to HEVC [10] or AV1 [11]. In [12], the authors evaluated the energy efficiency of AVC, HEVC, VP9, VVC, AV1, and AVM for available SW and HW decoders. Furthermore, the influence of SIMD instructions is evaluated for reference and optimized decoders. Another approach in [13] studied how the energy demand and the bit rate of AV1, VVC, VP9, and HEVC can be described by one metric. Thereby, a tradeoff between energy and bitrate is possible across multiple video coding standards. For HW decoder implementations, there are numerous challenges for AV1 and VVC for implementing new coding tools, as pointed

out in [14]. Also, the study in [15] assesses both video coding standards and shows that there is a significant demand for efficient algorithms and complexity reductions for new coding tools.

2) *Modeling*: The modeling of the video decoding energy was discussed in multiple papers. In [16], the authors modeled the energy demand of SW decoders by using PEs of the CPU using Valgrind. Alternatively, the usage of bit stream features was proposed in [17]–[20]. These models provide a high estimation accuracy. The energy demand of HW decoders was modeled using high-level information such as the video resolution [21].

In [22], the authors show that the power demand of the video streaming toolchain of mobile devices can be described accurately by high-level parameters such as the display brightness or the frame rate of the video sequence. The feature selection revealed that the display brightness, the frame rate, and the bit rate determine most of the energy demand of a mobile device during video streaming.

Finally, in [23], we presented a method to describe the HW decoder energy demand using SW profiling. The proposed models will be presented in detail in Section IV. However, the evaluated decoders were limited to HEVC and VP9, and the estimation error of the proposed method was over 10%, which will be improved significantly by the proposed methods in this work.

3) *Optimization*: In [24], the authors use bit stream features to train a model that describes the SW decoding energy demand. The corresponding model is used to extend the rate-distortion optimization of an HEVC encoder by the decoding energy demand. Thereby, the decoding energy demand is reduced significantly. Another approach is proposed in [25]–[27] that is based on a design space exploration. This approach evaluates the usage of coding tools in VVC in terms of bit rate and energy efficiency. Based on the optimization of this tradeoff, it selects whether a coding tool should be used or not. Thereby, energy demand reductions of up to 50% are achieved compared to the default VVC encoded bit streams. In [28], corresponding optimization opportunities are studied for VVC intra encoders. In [29], the preset selection is optimized by considering a balance of the encoding time, energy demand, and compression efficiency for HEVC encoders.

Typically, these optimizations are proposed for the reduction of SW decoding complexity. Our proposed method enables to extend the selection of new coding tools by the expected HW decoding energy consumption.

III. SETUP AND METRICS

In the following, we will explain the setup and the applied metrics of the paper. First, in Section III-A, we will discuss all video coding standards considered and show the corresponding SW encoder and decoder implementations. Then, we will show the encoding configurations and sequences used in the experiments. After that, we will introduce each evaluated measurement setup and the methodology of the corresponding energy measurements in Section III-B.

TABLE I

OVERVIEW OF ENCODER AND DECODER SW IMPLEMENTATIONS FOR EACH VIDEO CODING STANDARD. THE REFERENCE DECODER IMPLEMENTATION CORRESPOND TO THE SW THAT WAS USED DURING THE STANDARDIZATION PROCESS OF THE CORRESPONDING VIDEO CODING STANDARD. THE VERSION TAG OF THE CORRESPONDING SW IMPLEMENTATION IS GIVEN IN BRACKETS.

	Encoder	Reference Decoder	Optimized Decoder
AVC	x264 [30]	JM (19.1) [31]	FFmpeg (4.4) [32]
HEVC	x265 (3.5.1) [33]	HM (16.23) [34]	openHEVC (2.0) [35]
VVC	VVenC (1.7) [36]	VTM (19.0) [37]	VVdeC (1.6) [38]
VP9	libvpx (1.10) [39]	libvpx (1.10)	FFmpeg (4.4)
AV1	libaom (3.3) [40]	libaom (3.3)	dav1d (1.0) [41]
AVM	avm (3.0) [42]	avm (3.0)	/

A. Video Encoder and Decoder Setup

We evaluate 6 video coding standards. For each of those, we will show the encoder and decoder implementations used and discuss how the sequences are encoded. This work's oldest video coding standard is Advanced Video Coding (AVC), standardized in 2003 by ITU-T and ISO [43]. AVC is broadly used and HW implementations are available for most devices. For the encoding of the bit streams, we use x264 [30], as shown in Table I. For x264, we used the git version with hash ae03d92b. In the Table, we show the evaluated video coding standard in the first column and the used encoder with the corresponding SW version in the second column. The reference SW decoder implementation used and the optimized SW decoder are listed in the final two columns. We use two types of SW decoders since there are reference SW decoder implementations such as HM [34] that have not implemented SIMD instructions. Therefore, these decoders are not as optimized as the latest practical SW decoder implementations [41].

During the development of the specification, the reference SW of AVC was JM [31]. However, JM is not optimized by the Single Instruction Multiple Data (SIMD) instruction set and assembler optimizations, which are commonly used in SW decoders to reduce the complexity of the decoding process. Therefore, we also analyze the energy demand of an optimized decoder implementation, which is implemented into the FFmpeg framework [32].

After AVC, the next video coding format by ISO and ITU-T was High Efficiency Video Coding (HEVC), which was finalized in 2013 [44]. For encoding, we use the x265 software [33]. According to Table I, we use HM [34] as a reference decoder and openHEVC [35] as an optimized decoder implementation.

Finally, in 2020, with Versatile Video Coding (VVC), the latest video coding standard of ISO and ITU-T was published [45]. For VVC, we encode with the optimized implementation VVenC [46], accessed from [36]. As reference decoder implementation, we use VTM [37]. The optimized decoder of VVC is VVdeC [47].

With Alliance for Open Media (AOM), there is another standardization organization that aims to deploy an open and royalty-free video coding standard. In 2013, Google released the first version of the royalty-free VP9 [48] video coding standard. This was the predecessor of the AOMedia Video 1

(AV1) video coding format, which was standardized in 2018 [49]. For the encoding and decoding of VP9, we use libvpx [39]. As for AVC, we use FFmpeg as an optimized decoder. For AV1, we use libaom as an encoder and decoder [40], which was also the reference SW during the development of AV1. For the optimized AV1 decoder, we use dav1d [41].

Finally, there are efforts for the next video coding standard with AOM Video Model (AVM), which will be the successor of AV1 [42]. Therefore, we use the AVM SW to encode and decode video sequences. As the coding specification of AVM is still under development, there is no available optimized decoder yet. More details on each video coding standard can be found in [43]–[45], [48], [49].

With the previously mentioned encoders, we will encode video sequences according to the descriptions of the common test conditions (CTCs) of AOM [50]. From these CTCs, we take the video sequences of class A1 with 4K resolution, class A2 with full HD resolution, class A3 with HD resolution, and class B with full HD resolution. The sequences of class A1-3 show natural content, and the sequences of class B show synthetic screen content. Each sequence is encoded with the test conditions randomaccess (RA) and lowdelay B (LB) as described in the CTC [50]. In Table II, we show the commands used for each encoder in this work. Also, the quantization parameter (QP) values used for each test condition are given in the table. The sequence-specific parameters (e.g., resolution and frame rate) are left out since those depend on the properties of the corresponding video sequence.

For the decoders, we used three possibilities to turn SIMD instructions and assembler optimizations on and off: First, we could specify the SIMD instructions set with a decoder flag that enabled or disabled specific optimizations (e.g., with dav1d). Secondly, we changed the usage of macros associated with SIMD. Thereby, we could ignore the corresponding code parts during the compiling of the decoder binaries and decode without SIMD instructions (e.g., HM). Thirdly, we can specify the optimization options directly in a configuration file that is then used to compile the binaries (e.g., FFmpeg).

B. Measurement Setup

For the derivation of the decoding energy demand E_{decoding} , it is necessary to run two alternating measurements. First, the power demand during the decoding process P_{decoding} is measured and then, the power demand during idle P_{idle} . To get E_{decoding} , we calculate the following equation

$$E_{\text{decoding}} = \int_{t=t_0}^{t_0+T} P_{\text{decoding}}(t) dt - \int_{t=t_1}^{t_1+T} P_{\text{idle}}(t) dt, \quad (1)$$

where T corresponds to the duration of the decoding process that is also the measurement duration of P_{idle} .

In Figure 3, an example of those two measurements is shown, which was done on a single-board computer (SBC). In the graph, the red curve shows P_{decoding} and the blue curve shows P_{idle} . The decoding process in the red measurement takes from 1 to 2.4 seconds. The decoding energy demand E_{decoding} corresponds to the gray area in the graph and represents the difference between decoding and idle power.

TABLE II
SETTINGS OF EACH ENCODER FOR THE TEST CONDITIONS RANDOMACCESS (RA) AND LOWDELAY B (LB) ACCORDING TO THE AOM CTCs. THE USED QUANTIZATION PARAMETER (QP) VALUES ARE GIVEN FOR EACH TEST CONDITION.

Codec	Config.	Command	QP
x264	RA	--profile=high10 --preset=placebo --psnr --tune=psnr --no-scenecut --pass=1 --keyint=65	22 27 32 37 42 47
	LB	--profile=high10 --preset=placebo --psnr --tune=psnr --no-scenecut --pass=1 --keyint=infinite --min-keyint=-1	22 27 32 37 42 47
x265	RA	--profile=main10 -D=10 --preset=placebo --psnr --tune=psnr --pools --rd=6 --rect --amp pass=1 --frame-threads=1 --keyint=65 --min-keyint=65	22 27 32 37 42 47
	LB	--profile=main10 -D=10 --preset=placebo --psnr --tune=psnr --pools --rd=6 --rect --amp --pass=1 --frame-threads=1 --keyint=1	22 27 32 37 42 47
vvenc	RA	-c cfg/randomaccess_slower.cfg -rs 1 --qpa 1 --IntraPeriod=65	22 27 32 37 42 47
	LB	-c cfg/experimental/lowdelay_slower.cfg -rs 1 --qpa 1	22 27 32 37 42 47
libvpx	RA	--cpu-used=1 --passes=1 --lag-in-frames=19 --auto-alt-ref=1 --enable-tpl=0 --min-gf-interval=16 --max-gf-interval=16 --end-usage=q --kf-min-dist=65 --kf-max-dist=65 --profile=2 -b 10	23 31 39 47 55 63
	LB	--cpu-used=1 --passes=1 --lag-in-frames=0 --enable-tpl=0 --min-gf-interval=16 --max-gf-interval=16 --end-usage=q --kf-max-dist=9999 --kf-min-dist=9999 --profile=2 -b 10	23 31 39 47 55 63
libaom & avm	RA	--cpu-used=0 --passes=1 -b 10 --obu --lag-in-frames=19 --auto-alt-ref=1 --min-gf-interval=16 --max-gf-interval=16 --gf-min-pyr-height=4 --gf-max-pyr-height=4 --kf-min-dist=65 --kf-max-dist=65 --use-fixed-qp-offsets=1 --deltaq-mode=0 --enable-tpl-model=0 --end-usage=q --enable-keyframe-filtering=0	23 31 39 47 55 63
	LB	--cpu-used=0 --passes=1 -b 10 --obu --lag-in-frames=0 --min-gf-interval=16 --max-gf-interval=16 --gf-min-pyr-height=4 --gf-max-pyr-height=4 --kf-min-dist=9999 --kf-max-dist=9999 --use-fixed-qp-offsets=1 --deltaq-mode=0 --enable-tpl-model=0 --end-usage=q --enable-keyframe-filtering=0	23 31 39 47 55 63

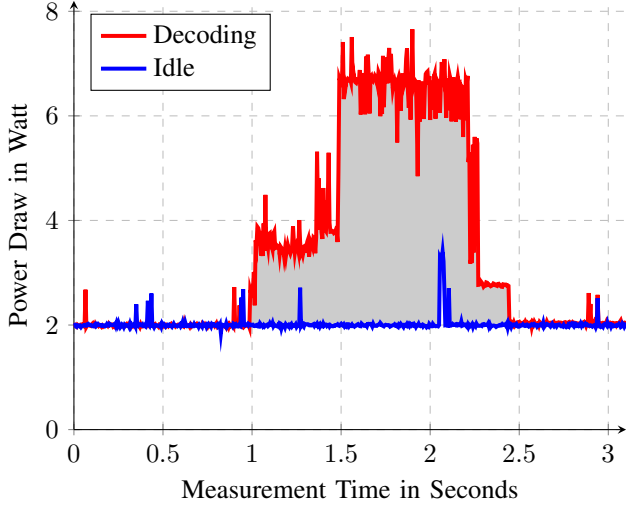


Fig. 3. Power measurement on the Rock Board with the external power meter. In the example, two separate measurement series are shown. The red curve shows the power draw of the board during the decoding of the bitstream, which starts in the curve at 1 second. The board uses the HW decoder chip, and the decoding process lasts until 2.4 seconds. The blue curve shows the energy demand during idle. The gray area illustrates the area between both curves and corresponds to the decoding energy demand E_{decoding} .

It is observed that the energy measurements are affected by noise. Thus, we check the statistical correctness of those measurements by a confidence interval test, as proposed in [18]. By doing so, the influence of noise on the measurements can be reduced. The statistical test is defined as follows

$$2 \cdot \frac{\sigma}{\sqrt{m}} \cdot t_{\alpha_{ci}}(m-1) < \beta_{ci} \cdot \overline{E_{\text{decoding}}}, \quad (2)$$

where σ denotes the standard deviation of the measurement series, m corresponds to the number of measurements that is at least five, and $\overline{E_{\text{decoding}}}$ is the arithmetic mean value of the decoding energy demand. The statistical coefficient

β_{ci} defines the maximum accepted deviation of the actual undistorted energy demand. The corresponding probability that the deviation of β_{ci} is not surpassed is given by α_{ci} . With $t_{\alpha_{ci}}$, the critical t-value of the Student's t-distribution is described. For the experiments, a β_{ci} of 0.02 and an α_{ci} of 0.99 is defined. This implies that with a probability of 99% the deviation of $\overline{E_{\text{decoding}}}$ is less than $\pm 2\%$ from the actual decoding energy demand.

In the following, we distinguish between two measurement setups that are similar to [23] and are built up as follows:

1) *Measurement Setup Software (MSS)*: We use a desktop PC with an internal power meter to measure the decoding energy demand of SW decoders. The desktop PC uses an Intel i7-8700 CPU with CentOS as the operating system. The integrated power meter on the CPU is called Running Average Power Limit (RAPL) [51]. The advantage of the power meter of RAPL is that it can be accessed by the operating system. In [52], it was shown that the measurement of RAPL highly correlates with the energy measurements of an external power meter.

2) *Measurement Setup Hardware (MSH)*: Secondly, the energy demand of HW decoder implementations is measured on the Rock 5 Model B single-board computer (SBC) by Radxa. This SBC provides an octa-core ARM processor with a quad-core Cortex-A76 and Cortex-A55 CPU [53]. Furthermore, the board supports a HW decoder implementation of the video coding standards AVC, HEVC, VP9, and AV1. As operating system, we use Ubuntu, and the HW decoder is accessed over FFmpeg. The decoding is processed without storing or displaying the decoded output. The power demand of the board is measured with the external high-precision power meter LMG611 by ZES Zimmer, which is connected to the main power supply jack of the SBC. Thereby, we measure the power demand of the entire board. However, since the constant power

draw of the board is subtracted by the idle measurement, we can still measure the additional energy demand of the decoding process itself. All used decoders are restricted to single-thread execution because some video decoders, such as JM and HM, cannot decode bit streams in multi-threading mode.

IV. LINEAR REGRESSION AND GAUSSIAN PROCESS REGRESSION

In the following, we will introduce two methods to train the parameters of the energy models. Therefore, this section will first explain the Linear Regression (LR) and then, the Gaussian process regression (GPR).

A. Linear Regression

According to [54], a linear regression can be defined as follows

$$Y = \beta_0 + \sum_{i=1}^N \beta_i \cdot X_i + \epsilon, \quad (3)$$

where Y denotes the output variable of the estimation, N corresponds to the set of features of the linear model, i is the index of the feature, X_i are the input variables, β_i are the unknown parameters of the model, and ϵ is the unknown error. We assume that the noise has a variance of σ_n^2 and a mean value of zero, which can be expressed by

$$\epsilon \sim \mathcal{N}(0, \sigma_n^2). \quad (4)$$

Thus, a linear model cannot derive a perfect estimation of the output variable \hat{Y} if the ground truth measurement of the output variable is affected by the noise factor ϵ .

For this work, the output variable of the regression in (3) is the decoding energy demand E_{decoding} . Thus, the goal of regression is to predict or estimate the decoding energy demand $\hat{E}_{\text{decoding}}$ as close as possible to E_{decoding} . Mathematically, the linear regression for the modeling of the decoding energy demand can also be described as follows

$$\hat{E}_{\text{decoding}} = \sum_{i \in \text{Features}} X_i \cdot e_i, \quad (5)$$

where i is the index of the feature, X_i is the number of occurrences of this specific feature i during the decoding process, and e_i is the specific energy demand of feature i that is necessary to process one instance of i . The energy coefficient e_i corresponds to the parameter β_i in (3). Thus, e_i reflects the energy demand required to process one instance of feature i . To derive the values of e_i , a least-square curve fitting algorithm based on a trust-region-reflective algorithm is utilized [55].

B. Gaussian Process Regression

As an alternative to the linear regression, the Gaussian process regression (GPR) can be utilized, which is a machine learning-based supervised training regression modeling [56]. As opposed to the parametric approach of the linear regression in (3), the Gaussian process regression is a non-parametric kernel-based probabilistic model. For the measurements, it is assumed that there is a Gaussian distributed error ϵ centered

around the medium measurement value of the measurement series (c.f., (4)). The linear regression would ideally be able to find an errorless solution in a noise-free measurement. However, with the measurement noise ϵ , this interferes with the curve fitting algorithm that cannot model the noise by linear coefficients.

According to [56], a Gaussian process (GP) is defined by

$$f(x) \sim \mathcal{GP}(m(x), k(x_s, x_t)), \quad (6)$$

where $m(x)$ corresponds to the mean function, x_s and x_t are two latent variables of the model, and $k(x_s, x_t)$ denotes the covariance or kernel function of the GP. In the following, an exponential kernel that is defined by the following covariance function is utilized

$$k(x_s, x_t) = \sigma_f^2 \exp\left(-\frac{|x_s - x_t|}{l}\right) + \sigma_n^2 \cdot \delta_{st}, \quad (7)$$

where δ_{st} corresponds to the Kronecker delta, l to the characteristic length scale, σ_f^2 to the variance of the function f , and σ_n^2 to the variance of the noise. Note that the last three mentioned parameters are variables that are trained as so-called hyperparameters [56]. Therefore, the Gaussian process regression can consider the variance of the introduced noise (c.f., (4)) as a trainable hyperparameter, which the kernel function can compensate. For the mean function $m(x)$, a linear function as in (3) is applied. To get an energy demand prediction with the GPR, the kernel function of the \mathcal{GP} is added in (6) to the basis functions of the linear regression in (3). Consequently, the following equation describes the energy demand of a video decoder

$$Y = f(x) + h(x)^\top \gamma, \quad (8)$$

where Y corresponds to the decoding energy demand (E_{decoding}), $f(x)$ to the kernel prediction in (6), and $h(x)^\top \gamma$ is defined as the basis function. This basis function can also be expressed by using the linear model in (3) and (5), as follows

$$h(x)^\top \gamma = \beta_0 + \sum_{i=1}^N \beta_i \cdot X_i = \sum_{i \in \text{Features}} X_i \cdot e_i. \quad (9)$$

Thus, $h(x)$ corresponds to the feature vector X (c.f., (5)) and γ corresponds to the set of trained feature coefficients e (c.f., (5)). In summary, the Gaussian process regression adds a kernel function to the linear regression, which helps to model the basic functions despite the problem of uncertainty through noise. For the training of the GPR's hyperparameters, the *fitrgp* implementation of Matlab [57] is utilized. A more detailed description of the Gaussian process regression can be found in [56].

For the evaluation of the estimation accuracy, the mean average percentage error (MAPE) $\bar{\epsilon}$ is utilized that is described by

$$\bar{\epsilon} = \frac{1}{M} \sum_{i=1}^M \frac{|E_{\text{decoding},i} - \hat{E}_{\text{decoding},i}|}{E_{\text{decoding},i}}, \quad (10)$$

where M corresponds to the number of measured samples in the evaluated data set, i to the index of the measurement in the data set, $E_{\text{decoding},i}$ to the measured energy demand of bit

stream i , and $\hat{E}_{\text{decoding},i}$ to the corresponding estimation of the energy demand. Therefore, a lower value of $\bar{\varepsilon}$ corresponds to a higher accuracy of the energy model.

In addition to a low estimation error, it is important to ensure that the data of the training and the validation are separated for the linear and Gaussian process regression. Otherwise, there is a risk of overfitting towards the training data, which leads to a higher estimation error if the model is applied to a different data set [58]. Thus, we will use 10-fold cross validation for the SW and HW decoding energy modeling.

C. Energy Models

For the energy modeling, we will evaluate the following three models:

1) *Temporal Energy Model*: For the temporal energy model, we utilize the decoding time of a SW decoder $t_{\text{dec},\text{SW}}$ to estimate and predict the decoding energy demand $\hat{E}_{\text{decoding}}$ of a SW and HW decoder as follows

$$\hat{E}_{\text{decoding}} = t_{\text{decoding},\text{SW}} \cdot P + E_{\text{offset}}. \quad (11)$$

The regressions have to train the following two parameters: the constant power draw P and the energy offset of the decoding process E_{offset} .

For standardization, the SW decoding time is often utilized to describe the complexity of a video decoder. Consequently, we assume the temporal energy model is the state-of-the-art estimation for the video decoder complexity. Therefore, we benchmark our findings to the temporal model.

2) *Perf Energy Model*: As suggested by AOM CTC, we use Perf to measure the SW decoder complexity. Perf is a tool in the Linux kernel that can report different kinds of PEs, such as the instruction count or reads to the memory. The PEs are derived by utilizing the HW counters on the CPU. Thereby, Perf can evaluate the performance and identify bottlenecks of the SW without a temporal overhead. The recommendation of AOM is to report the instruction count, the cycle count, and the user time for newly proposed coding tools. In the following, we will use these three features as the 'Perf CTC' model as recommended in [23].

3) *Valgrind Energy Model*: Next to the first two models, we use Valgrind [8] to describe the decoding process by PEs that comprise the necessary CPU instruction types. Valgrind is simulating a machine with two levels of cache: first-level (L1) and last-level cache (LLC).

In this work, we evaluate the 13PE model proposed in [23]. In Table III, a list of PEs is provided along with a short description. The conditional branches describe a jump resulting from a comparison, such as in an if-statement. An instruction pointer describes an indirect branch to an address in the memory that contains a destination address for the jump.

With the following command, we derive the features of the Valgrind model:

```
valgrind --tool=callgrind --simulate-cache=yes
--dump-instr=yes --collect --jumps=yes
--branch=yes --I1=32768,8,64 --D1=32768,8,64
--LL=12582912,24,64 [decoder command]
```

TABLE III
LIST OF PEs THAT ARE PROFILED WITH VALGRIND. A SHORT DESCRIPTION OF EACH PE IS PROVIDED.

Short	PEs
Ir	I cache reads (number of executed instructions)
Dr	D cache reads (data memory reads)
Dw	D cache writes (data memory writes)
I1mr	I1 cache read misses
D1mr	D1 cache read misses
D1mw	D1 cache write misses
ILmr	LLC instruction read misses
DLmr	LLC data read misses
DLmw	LLC data write misses
Bc	Conditional branches executed
Bcm	Conditional branches mispredicted
Bi	Indirect branches executed
Bim	Indirect branches mispredicted

By using the option `simulate-cache`, it is possible to simulate the cache behavior and count cache misses, read accesses, and write accesses to memory [8]. Consequently, the first 9 features of Table III can be derived by using this option. With `collect-jumps`, the SW profiling can count conditional jumps, and with `branch-sim`, the features associated with branches can be counted. If I1 (level 1 instruction cache), D1 (level 1 data cache), and LL (last-level cache) are specified, it is possible to get reproducible results on different machines that run Valgrind. The parameters of the options reflect the settings of the Intel i7-8700 CPU on the desktop PC. The first value of each defines the size of the corresponding cache, the second value is the associativity size, and the third value is the line size of the cache.

V. SOFTWARE ENERGY MODELING

In the following, we will discuss the energy models introduced in the previous section for SW video decoders. First, we will evaluate the results using linear regression and then, show the results using the GPR.

In Table IV, LR and GPR are evaluated in terms of the MAPE from (10). In the first column, we show the corresponding SW decoder that is evaluated. We distinguish between the decoder version with SIMD instructions enabled or disabled. We average the results of all SW decoders in the final row. For each decoder, we evaluate the following models from Section IV: Temporal, Perf CTC, and Valgrind 13PE. The table's MAPE $\bar{\varepsilon}$ shows that all SW decoders can be modeled with an average error below 2.5%. The Temporal model has the lowest estimation error $\bar{\varepsilon}$ with 1.33%, followed by the Valgrind 13PE model with 1.47%. This shows that each energy model is suitable to accurately describe the complexity of a SW decoder in terms of energy demand.

Table IVb shows the same evaluations for the GPR. Again, all energy models have an estimation errors of less than 2% showing that each set of features is suitable to model SW decoders with the GPR. We determine that the Valgrind 13PE has the lowest $\bar{\varepsilon}$ of 1.25% on average, followed by the temporal model that has a $\bar{\varepsilon}$ of 1.45%. The highest error on average can be found with the Perf CTC model, which has a $\bar{\varepsilon}$ of 1.73%. Furthermore, we take those average values as a lower bound

TABLE IV
MAPE RESULTS OF THE SW DECODER ENERGY DEMAND MODELING. THE LOWEST $\bar{\varepsilon}$ FOR EACH DECODER IS GIVEN IN BOLD.

Software Decoder	Temporal	Perf CTC	Valgrind 13PE
AVC	JM	2.10%	1.50%
	FFmpeg	6.28%	5.51%
	FFmpeg SIMD off	2.82%	2.41%
HEVC	HM	0.68%	0.87%
	openHEVC	0.73%	1.28%
	openHEVC SIMD off	0.57%	0.93%
VP9	libvpx	0.99%	1.04%
	libvpx SIMD off	0.52%	0.80%
	FFmpeg	0.93%	1.26%
	FFmpeg SIMD off	0.42%	0.97%
AV1	libaom	0.96%	1.04%
	libaom SIMD off	0.77%	1.01%
	dav1d	0.87%	1.36%
	dav1d SIMD off	0.84%	0.95%
VVC	VTM	0.71%	1.63%
	VTM SIMD off	1.25%	1.27%
	VVdeC	1.68%	1.49%
	VVdeC SIMD off	1.35%	1.40%
AVM	AVM	1.29%	1.61%
	AVM SIMD off	0.84%	1.02%
Average	1.33%	2.45%	1.47%

(a) Linear Regression

Software Decoder	Temporal	Perf CTC	Valgrind 13PE
AVC	JM	2.12%	1.48%
	FFmpeg	6.99%	5.41%
	FFmpeg SIMD off	2.82%	2.48%
HEVC	HM	0.68%	0.63%
	openHEVC	0.86%	0.77%
	openHEVC SIMD off	0.62%	0.66%
VP9	libvpx	1.33%	0.77%
	libvpx SIMD off	0.46%	0.50%
	FFmpeg	1.18%	0.84%
	FFmpeg SIMD off	0.57%	0.63%
AV1	libaom	1.45%	0.88%
	libaom SIMD off	0.72%	0.76%
	dav1d	1.05%	0.93%
	dav1d SIMD off	0.79%	0.73%
VVC	VTM	0.85%	1.59%
	VTM SIMD off	1.18%	1.17%
	VVdeC	1.62%	1.06%
	VVdeC SIMD off	1.30%	1.01%
AVM	AVM	1.53%	1.28%
	AVM SIMD off	0.83%	0.88%
Average	1.45%	1.73%	1.25%

(b) Gaussian Process Regression

of the prediction accuracy for the hardware decoder modeling and cross-codec prediction. The direct comparison of LR and GPR shows that we have no significant differences in terms of estimation accuracy for SW decoding energy modeling. Consequently, both types of regression are suitable for SW energy modeling.

VI. HARDWARE ENERGY MODELING

In the following, we will discuss the HW decoder modeling results, as pointed out in the left block (training) in Figure 2. Therefore, we take the SW decoders' profiling and decoding time measurement to estimate the HW decoder's energy demand. First, we will review the results of the LR and then, show the results with the GPR.

Table Va shows each model's MAPE $\bar{\varepsilon}$ and evaluated decoder version using LR. We determine that the $\bar{\varepsilon}$ for HW decoder modeling is significantly higher than for the SW decoder modeling in Table IVa. Specifically, the Temporal model has an increased $\bar{\varepsilon}$ of 18.65% on average for all decoders (c.f., Table Va with 1.33%). The Perf CTC model has an even higher $\bar{\varepsilon}$ of 26.12% (c.f., Table Va with 2.45%). As a result, neither model yields sufficient accuracy with the LR for modeling the energy demand of HW decoders. For the 13PE Valgrind model, we have a $\bar{\varepsilon}$ of 5.27%.

By replacing the LR with the GPR, it is shown in Table Vb that significantly lower $\bar{\varepsilon}$ are reachable. However, the Temporal model still has a $\bar{\varepsilon}$ of 17.12% utilizing the GPR. Based on this, we conclude that the SW decoding time is not suitable to predict the HW decoder complexity. Also, the Perf CTC model has significantly higher $\bar{\varepsilon}$ of 10.01%. For the 13PE model, we derive a $\bar{\varepsilon}$ of 1.79%, which is close to the estimation error that was observed for the SW decoder modeling in Table IVb. Thereby, we show that we can reduce the estimation error

by more than half by changing the type of regression from LR to GPR, such that we only use GPR for the subsequent considerations.

VII. HARDWARE ENERGY CROSS-CODEC PREDICTION FOR UNKNOWN HARDWARE DECODERS

Finally, we show a methodology that predicts the complexity of an unknown HW decoder implementation as shown by the middle box in Figure 2. Therefore, we use a video coding standard with an existing HW and SW implementation for the training of the energy models. For the verification, the energy consumption of another standard's hardware decoder is estimated. However, only the corresponding SW decoder was used for the estimation of the HW decoding energy demand. For example, we assume that AVC can cross-codec predict HEVC and VP9, and AV1 can be cross-codec predicted by AVC, HEVC, and VP9.

A. Linear Transformation for Verification

According to Figure 2, we first train the energy models with Codec A. Then, we use the SW profiling of Codec B to get the energy cross-codec prediction of \hat{E}_{cross} . Those are derived by using the energy models that were trained with the cross-codec prediction energy demand of the LR or GPR. In Table VI, we list all decoders and combination of video decoders that we used for the training. In the following, we define each training option to be a phase. In phases 1-3, we use a single video decoder to train the coefficients of the GPR or LR, as shown in the second column of the table. In phases 4-7, we combine the data sets of multiple video decoders for the modeling of the training. In the third column, we denote the decoders that are verified in each phase.

TABLE V
MAPE RESULTS OF THE HW DECODER ENERGY DEMAND MODELING. THE LOWEST $\bar{\epsilon}$ FOR EACH DECODER IS GIVEN IN BOLD.

Software Decoder	Temporal	Perf CTC	Valgrind 13PE
AVC	JM	15.83%	3.70%
	FFmpeg	20.04%	3.77%
	FFmpeg SIMD off	17.72%	3.68%
HEVC	HM	21.03%	2.74%
	openHEVC	24.66%	4.02%
	openHEVC SIMD off	19.51%	4.57%
VP9	libvpx	21.10%	5.50%
	libvpx SIMD off	14.89%	5.53%
	FFmpeg	21.86%	3.65%
	FFmpeg SIMD off	15.47%	3.42%
AV1	libaom	16.86%	7.68%
	libaom SIMD off	18.04%	10.60%
	dav1d	16.10%	6.66%
	dav1d SIMD off	17.95%	8.27%
Average	18.65%	26.12%	5.27%

(a) Linear Regression

Software Decoder	Temporal	Perf CTC	Valgrind 13PE
AVC	JM	12.16%	2.53%
	FFmpeg	19.82%	2.52%
	FFmpeg SIMD off	14.97%	2.55%
HEVC	HM	14.31%	0.98%
	openHEVC	22.32%	0.86%
	openHEVC SIMD off	14.28%	0.84%
VP9	libvpx	19.76%	0.93%
	libvpx SIMD off	13.61%	0.83%
	FFmpeg	20.10%	1.25%
	FFmpeg SIMD off	14.39%	0.84%
AV1	libaom	20.59%	2.82%
	libaom SIMD off	16.70%	2.81%
	dav1d	19.35%	2.46%
	dav1d SIMD off	17.31%	2.78%
Average	17.12%	10.01%	1.79%

(b) Gaussian Process Regression

TABLE VI

OVERVIEW OF THE CROSS-CODEC PREDICTION PHASES. IN THE SECOND COLUMN, WE DENOTE THE VIDEO CODING STANDARDS THAT ARE USED TO TRAIN THE ENERGY MODELS WITH THE GPR. IN THE THIRD COLUMN, WE SHOW THE VIDEO CODING STANDARDS THAT ARE VERIFIED BY THE CORRESPONDING TRAINING.

Phase	Training (Codec A)	Verification (Codec B)
Phase 1	AVC	HEVC
		VP9
		AV1
Phase 2	HEVC	AV1
Phase 3	VP9	AV1
Phase 4	AVC + HEVC	AV1
Phase 5	AVC + VP9	AV1
Phase 6	AVC + HEVC + VP9	AV1
Phase 7	HEVC + VP9	AV1

In Figure 4, we show two examples of the cross-codec prediction with the Perf CTC model (a) and the Valgrind 13PE model (b). The horizontal axis shows the ground truth energy measurement of the AV1 HW decoder, and the vertical axis shows the energy demand cross-codec prediction trained with HEVC and VP9 (phase 7). Both axes are given in Joule. Each marker corresponds to one bit stream of the data set. The green markers show the estimated energy demand \hat{E}_{cross} of the GPR with the pre-trained energy models. In Figure 4b, we observe that the HW measurement of codec B has a high correlation with \hat{E}_{cross} . However, the correlation is significantly lower for the estimation in Figure 4a.

For a description of the linear relationship of \hat{E}_{cross} and E_{veri} , we utilize the Pearson correlation coefficient (PCC) R that measures the linear association of both [59]. Additionally, the coefficient of determination R^2 can be calculated to derive the proportion of the variables' variation that can be explained by the independent variable [59]. The PCC R values are shown in Table VII. In the Table, S.d. indicates that SIMD is disabled. We observe that the Valgrind 13PE model has consistent values of above 0.82 for the optimized decoders. Correspondingly, we get a R^2 value of 0.67. Thus, more

TABLE VII

ANALYSIS OF PEARSON'S CORRELATION COEFFICIENT (PCC) R FOR THE VERIFICATION VIDEO DECODER ENERGY MEASUREMENTS E_{VERI} AND THE CROSS-CODEC PREDICTION ENERGY DEMAND \hat{E}_{CROSS} . HIGHEST VALUES ARE HIGHLIGHTED IN BOLD.

Training	SW Profiling Verification	Temp.	Perf CTC	Valgrind 13PE
Phase 1 AVC	HEVC Ref.	0.75	0.74	0.73
	HEVC Opt.	0.63	0.83	0.90
	HEVC Opt. S.d.	0.83	0.85	0.79
	VP9 Ref.	0.75	0.69	0.96
	VP9 Ref. S.d.	0.89	0.87	0.96
	VP9 Opt.	0.71	0.47	0.97
	VP9 Opt. S.d.	0.88	0.78	0.94
	AV1 Ref.	0.72	0.66	0.77
	AV1 Ref. S.d.	0.87	0.89	0.60
	AV1 Opt.	0.77	0.68	0.82
AV1 Opt. S.d.	0.84	0.82	0.22	
Phase 2 HEVC	AV1 Ref.	0.74	0.25	0.96
	AV1 Ref. S.d.	0.87	0.90	0.92
	AV1 Opt.	0.73	0.54	0.98
Phase 3 VP9	AV1 Opt. S.d.	0.81	0.77	0.98
	AV1 Ref.	0.79	0.78	0.96
	AV1 Ref. S.d.	0.87	0.89	0.81
Phase 4 AVC+HEVC	AV1 Opt.	0.78	0.79	0.93
	AV1 Opt. S.d.	0.81	0.77	0.02
	AV1 Ref.	0.75	0.65	0.89
Phase 5 AVC+VP9	AV1 Ref. S.d.	0.87	0.90	0.89
	AV1 Opt.	0.73	0.57	0.98
	AV1 Opt. S.d.	0.82	0.78	0.87
Phase 6 AVC+VP9+HEVC	AV1 Ref.	0.67	0.35	0.75
	AV1 Ref. S.d.	0.87	0.89	0.71
	AV1 Opt.	0.77	0.73	0.95
Phase 7 HEVC+VP9	AV1 Opt. S.d.	0.84	0.80	0.82
	AV1 Ref.	0.76	0.28	0.88
	AV1 Ref. S.d.	0.87	0.89	0.85
Phase 7 HEVC+VP9	AV1 Opt.	0.75	0.61	0.97
	AV1 Opt. S.d.	0.82	0.78	0.95
	AV1 Ref.	0.75	0.51	0.97
Phase 7 HEVC+VP9	AV1 Ref. S.d.	0.87	0.88	0.83
	AV1 Opt.	0.75	0.64	0.99
	AV1 Opt. S.d.	0.81	0.76	0.93

than 67% of the variance of E_{veri} can be explained by a linear model with \hat{E}_{cross} . By combining multiple video coding standards to train the optimized decoders (phases 4-7), we get a PCC of over 0.95 for the 13PE Valgrind model. Furthermore, for phase 7, the PCC value of \hat{E}_{cross} and E_{veri} is 0.99. Consequently, there is a very high correlation in phase 7, which indicates a strong relationship between the cross-codec prediction and the ground truth energy measurement. As the correlation coefficients are invariant to linear transformation [60], we propose to compensate this scaling of the energy demand prediction by a first-order linear transformation. This transformation is described by the following equation:

$$\hat{E}_{\text{veri}} = \alpha + \hat{E}_{\text{cross}} \cdot \beta, \quad (12)$$

which linearly scales \hat{E}_{cross} with a factor β and adds an offset α . Both parameters are trained with a LR to fit the actual energy measurement of codec B. It is important to note that β is influenced by the technology node, by the implementation efficiency, and by the throughput. Each of those exemplary factors has direct influence on the HW energy efficiency. These factors are unknown during the standardization and only assumptions can be made. With α , we introduce an offset that represents changes in terms of static energy, which can be attributed to the complexity of the initialization process in software (e.g., drivers).

In Figure 4, the red markers show the linearly scaled energy demand \hat{E}_{cross} . Ideally, the cross-codec prediction matches the measurement shown by the red dashed line. In Figure 4b, it can be seen that estimated and measured energy consumptions have a high linear correlation. With the linear transformation, \hat{E}_{veri} is close to the dashed ideal line.

During the standardization, it would not be possible to train α and β because a hardware implementation is not available. Therefore, we cannot evaluate the accuracy of the predicted energy demand \hat{E}_{cross} since the corresponding absolute energy demand of an unknown video decoder implementation is not yet available. Furthermore, there is usually a significant improvement of the technology node over time between two iterations of video coding standards. However, we cannot incorporate those improvements into the model. Nevertheless, we can still evaluate the relative influence of processing complexities on the energy efficiency of an unknown HW decoder implementation. Note that SW complexities of new tools are reported and evaluated in the same manner.

B. Verification of Cross-Codec Prediction

As shown in the right box in Figure 2, in the verification, we predict the HW decoding energy demand of a coding standard, which is not part of the training. Furthermore, we use a linear transformation to compare the predicted energy demand of the GPR \hat{E}_{cross} with the actual measurement of the HW decoder. As we want to verify if these models are sufficiently accurate, we must utilize an existing HW decoder implementation, exclude the evaluated coding standard from the training, and assess if the measurements match. An example would be to use the HW decoding measurements and SW decoding profiling of HEVC and VP9 to train the energy models. Then, we use the SW profiling of AV1 to cross-predict the HW energy demand.

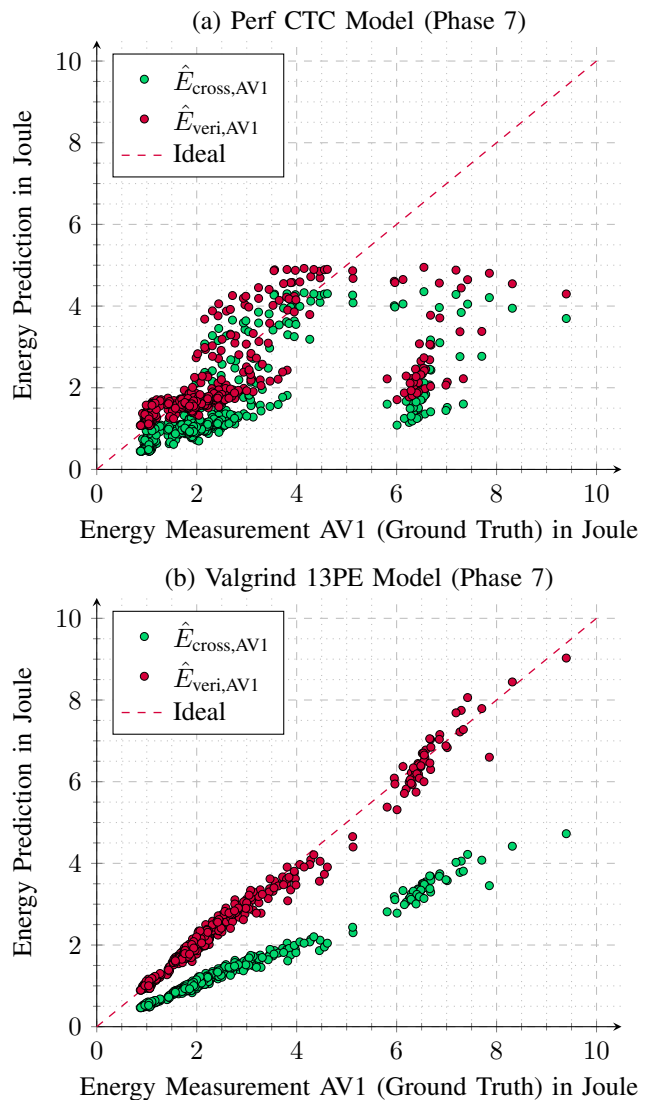


Fig. 4. Evaluation of the cross-codec prediction accuracy for the Perf CTC (a) and Valgrind 13PE (b) model. In both subfigures, the vertical axis denotes the energy demand prediction of the HW decoder, and the horizontal axis shows the corresponding measurement. Each marker corresponds to one bitstream of the AV1 set. The green markers show the initial decoding energy cross-codec prediction $\hat{E}_{\text{cross,AV1}}$ with the GPR, and the red markers show the linearly transformed energy demand of the verification $\hat{E}_{\text{veri,AV1}}$. The red dashed line corresponds to the case that the energy demand cross-codec prediction matches the corresponding measurement.

In Tables VIIIa and VIIIb, we provide the results of the verification. Therefore, we predict the complexity of a newer video coding standard by the modeling of the HW implementation of an older coding standard and the SW profiling of the new coding standard. The first column lists all video coding standards used to train the GPR models, and the second column states which SW decoder and video coding standard are used for the verification. Note that in Table VIIIa, the video decoders with SIMD instructions and enabled are evaluated, and in Table VIIIb, the corresponding decoders with SIMD instructions disabled. In Table VIIIa, we will first analyze the case in which a single video coding standard is used for the training. This corresponds to the results from phases 1-3.

When training with AVC (Phase 1), we determine that all

TABLE VIII

ANALYSIS OF THE MAPE FOR THE VERIFICATION OF THE CROSS-CODEC PREDICTION. THE FIRST COLUMN SHOWS THE VIDEO CODING STANDARDS USED FOR THE TRAINING OF THE GPR. IN THE SECOND COLUMN, WE LIST THE SW DECODER THAT IS UTILIZED FOR THE PROFILING OF THE DECODING PROCESS, WHICH IS THEN USED FOR THE CROSS-CODEC PREDICTION. THE LOWEST $\bar{\varepsilon}$ FOR EACH DECODER IS GIVEN IN BOLD.

Training	SW Prof. Verification	Temp.	Perf CTC	Valgrind 13PE
Phase 1 AVC	HM	26.68%	26.80%	24.89%
	openHEVC	27.34%	24.73%	18.28%
	libvpx	19.25%	24.14%	13.52%
	FFmpeg	25.87%	27.90%	16.72%
	libaom dav1d	20.50% 22.18%	23.05% 22.26%	20.11% 19.00%
Phase 2 HEVC	libaom	19.48%	28.10%	10.17%
	dav1d	22.08%	24.81%	8.04%
Phase 3 VP9	libaom	20.24%	21.51%	9.18%
	dav1d	19.83%	16.25%	11.85%
Phase 4 AVC,HEVC	libaom	18.64%	24.98%	14.55%
	dav1d	22.77%	24.26%	8.24%
Phase 5 AVC,VP9	libaom	27.26%	31.82%	14.95%
	dav1d	20.29%	20.04%	9.34%
Phase 6 AVC,HEVC,VP9	libaom	22.86%	32.46%	13.30%
	dav1d	21.07%	23.43%	7.07%
Phase 7 HEVC,VP9	libaom	22.49%	28.90%	10.43%
	dav1d	21.40%	23.03%	4.54%

(a) SIMD enabled

Training	SW Prof. Verification	Temp.	Perf CTC	Valgrind 13PE
Phase 1 AVC	HM	26.68%	26.80%	24.89%
	openHEVC	25.32%	24.11%	22.90%
	libvpx	20.92%	22.41%	12.79%
	FFmpeg	23.41%	25.37%	26.45%
	libaom dav1d	18.13% 19.10%	18.45% 20.69%	17.27% 31.50%
Phase 2 HEVC	libaom	19.43%	17.42%	15.68%
	dav1d	23.34%	22.34%	7.81%
Phase 3 VP9	libaom	18.09%	19.40%	11.29%
	dav1d	22.59%	23.95%	15.18%
Phase 4 AVC,HEVC	libaom	18.86%	17.66%	15.93%
	dav1d	31.34%	21.46%	16.08%
Phase 5 AVC,VP9	libaom	17.42%	16.89%	19.32%
	dav1d	20.36%	22.25%	15.92%
Phase 6 AVC,HEVC,VP9	libaom	18.33%	16.40%	17.99%
	dav1d	21.78%	22.55%	9.91%
Phase 7 HEVC,VP9	libaom	18.28%	17.19%	20.32%
	dav1d	23.05%	23.71%	13.54%

(b) SIMD disabled

models have a significantly higher $\bar{\varepsilon}$ than 10% when predicting the energy demand of HEVC, VP9, and AV1. With Valgrind, we determine significantly lower cross-codec prediction errors. The high error values indicate that AVC cannot accurately cross-codec predict the HW decoder energy demand of another video coding standard.

The cross-codec prediction accuracy for AV1 is significantly enhanced if HEVC (Phase 2) or VP9 (Phase 3) replace AVC. For the optimized decoders, we determine that the 13PE model has an error of 11.85% with the training on VP9 and of 8.04% on HEVC. In the Table, we also found that the Temporal model has a $\bar{\varepsilon}$ of over 20% on average. The Perf CTC model has mostly higher $\bar{\varepsilon}$ values in comparison with the Temporal model. Consequently, the proposed models are significantly better at predicting the energy demand of an

unknown HW decoder implementation than the decoding time or the proposed metrics of the AOM CTC.

The higher $\bar{\varepsilon}$ of AVC indicates that the generation of the video coding standards plays an essential role in the accuracy of the cross-codec predictions. As AVC was standardized in 2003, it is ten years older than VP9 and HEVC. Since then the computational capabilities increased significantly. This made it possible for standardization bodies to incorporate more sophisticated coding tools and more complex partitioning schemes into video coding standards. Thereby, the HW implementations also became more versatile. As a consequence, AVC is not a valid representative for modern video coding standards.

In the following, we improve the cross-codec prediction by merging two or more video coding standards and train one model with multiple video coding standards. The goal is to predict the AV1 decoding energy demand accurately. By combining AVC and HEVC (Phase 4), we get a $\bar{\varepsilon}$ of 8.24% with the Valgrind 13PE model for the optimized decoders. If AVC and VP9 (Phase 5) are combined, we get similar results. The combination of the video coding standards AVC, HEVC, and VP9 (Phase 6) for the training of the Valgrind 13PE model yields a $\bar{\varepsilon}$ of 7.07% for the optimized decoders. Unfortunately, the reference decoders are not able to achieve similar results. We assume that the lack of SIMD instructions and assembler optimizations in HEVC and AVC reference implementations limits the capabilities to predict AV1.

Finally, we evaluate the usage of VP9 and HEVC (Phase 7) to train the models, which improves $\bar{\varepsilon}$ significantly. For the Valgrind 13PE model, we get a $\bar{\varepsilon}$ of 4.54%. This is significantly lower than for the Perf CTC model with a $\bar{\varepsilon}$ of 23.03%. In Figure 4, we show the results of this evaluation. In Figure 4a, we show the cross-codec prediction with the Perf CTC model, and in Figure 4b, for the Valgrind 13PE model. In Figure 4a, we determine that the energy cross-codec prediction is distributed broadly with high estimation errors, and the linear transformation cannot compensate for the inaccuracies. Therefore, if the complexity report that AOM suggests is utilized, we determine that the estimation accuracy of the cross-codec prediction of a HW decoder energy demand is insufficient with our proposed framework. However, with the proposed Valgrind 13PE model, we can reduce this uncertainty significantly. Therefore, we propose this methodology to predict the energy demand of an unknown HW video decoder implementation.

Table VIIIb shows the evaluation results if the decoders do not use SIMD instructions. The cross-codec prediction accuracy is significantly lower than the results in Table VIIIa. Consequently, we recommend to use decoders with SIMD instructions to cross-codec predict the HW energy demand.

In summary, we had the following findings in our work:

- SW decoding energy modeling has estimation errors below 2% on average using SW profiling.
- SW decoding time is not suitable for the prediction of the HW decoding energy demand.
- SW profiling can be used to predict relative differences in HW energy consumption for an unknown implemen-

tation.

- In the best case using the 13PE Valgrind model, we reach estimation errors below 5% when training with optimized SIMD decoders of the coding standards HEVC and VP9.
- It is better to use more recent coding standards for training.

VIII. CONCLUSION

We found that the complexity of a HW decoder implementation was often neglected during the development of a video coding standard. In this work, we provided a HW decoding energy metric that can be used in standardization to amend the adoption of compression technologies by incorporating the predicted HW energy complexity into the consideration. We show that the processor-events based 13PE model has a MAPE of 1.79% for the estimation of HW decoders and a MAPE of 1.25% for SW decoders. Moreover, the developed metric allows to cross-codec predict the energy demand of an unknown HW implementation with a MAPE of 4.54% without using the corresponding HW decoder for training.

The proposed methodology will help standardization bodies develop future video coding standards with better HW energy efficiency, leading to reduced GHG emissions and longer battery life for mobile devices. We showed that AVC, HEVC, VP9 reference software could have predicted AV1 VLSI decoder energy demand with an error of 4.54% during its standardization process. This provides evidence that AVC, HEVC, VP9, AV1 reference software can be used to accurately predict VLSI decoder energy demand of the AVM coding standard which is being standardized currently. Consequently, the standardization process can use such predictions to select coding standard algorithms with lower energy demand, which may also lead to a smaller area.

In future work, we aim to investigate the differences between reference and optimized decoder implementations to improve cross-codec prediction accuracy. Additionally, we plan to evaluate coding tools. Also, we like to study the capabilities to predict encoder implementations. The proposed methodology could be used for other algorithms, where both SW and HW is available with the same functionality. Results indicate that this method can potentially be generalized to other types of algorithms.

REFERENCES

- [1] Ericson. (2023, Jun.) Ericson mobility report. [Online]. Available: <https://www.ericsson.com/49dd9d/assets/local/reports-papers/mobility-report/documents/2023/ericsson-mobility-report-june-2023.pdf>
- [2] M. Efoui-Hess. (2019, Jul.) Climate crisis: The unsustainable use of online video. The practical case for digital sobriety. [Online]. Available: <https://theshiftproject.org/en/article/unsustainable-use-online-video/>
- [3] C. Herglotz, M. Kränzler, R. Schober, and A. Kaup, "Sweet streams are made of this: The system engineer's view on energy efficiency in video communications," *IEEE Circuits and Systems Magazine*, vol. 23, no. 1, pp. 57–77, April 2023.
- [4] C. Herglotz, S. Coulombe, S. Vakili, and A. Kaup, "Power modeling for virtual reality video playback applications," in *Proc. IEEE International Symposium on Consumer Technology (ISCT)*, Ancona, Italy, Jun. 2019.
- [5] M. Kränzler, C. Herglotz, and A. Kaup, "A comparative analysis of the time and energy demand of versatile video coding and high efficiency video coding reference decoders," in *Proc. IEEE International Workshop on Multimedia Signal Processing (MMSp)*, Tampere, Finland, Sep. 2020.
- [6] G. Bjøntegaard, "Calculation of average PSNR differences between RD curves," Austin, TX, USA, document, VCEG-M33, Jan. 2001.
- [7] C. Herglotz, H. Och, A. Meyer, G. Ramasubbu, L. Eichermüller, M. Kränzler, F. Brand, K. Fischer, D. T. Nguyen, A. Regensky, and A. Kaup, "The bjøntegaard bible – why your way of comparing video codecs may be wrong," *IEEE Transactions on Image Processing*, vol. 33, pp. 987–1001, 2024.
- [8] Valgrind. Accessed 2021-10-01. [Online]. Available: <https://valgrind.org/>
- [9] T. Laude, Y. G. Adhisantoso, J. Voges, M. Munderloh, and J. Ostermann, "A comprehensive video codec comparison," *APSIPA Transactions on Signal and Information Processing*, vol. 8, no. 1, 2019.
- [10] A. Mercat, A. Makinen, J. Sainio, A. Lemmetti, M. Viitanen, and J. Vanne, "Comparative rate-distortion-complexity analysis of VVC and HEVC video codecs," *IEEE Access*, vol. 9, pp. 67 813–67 828, 2021.
- [11] T. Nguyen and D. Marpe, "Compression efficiency analysis of AV1, VVC, and HEVC for random access applications," *APSIPA Transactions on Signal and Information Processing*, vol. 10, no. 1, 2021.
- [12] M. Kränzler, A. Kaup, and C. Herglotz, "A comprehensive review of software and hardware energy efficiency of video decoders," in *Proc. for Picture Coding Symposium (PCS)*, Taichung, Taiwan, 6 2024.
- [13] A. Katsenou, J. Mao, and I. Mavromatis, "Energy-rate-quality tradeoffs of state-of-the-art video codecs," in *Proc. Picture Coding Symposium (PCS)*, San Jose, CA, USA, Dec. 2022.
- [14] M. Correa, M. Saldanha, A. Borges, G. Correa, D. Palomino, M. Porto, B. Zatt, and L. Agostini, "AV1 and VVC video codecs: Overview on complexity reduction and hardware design," *IEEE Open Journal of Circuits and Systems*, vol. 2, pp. 564–576, 2021.
- [15] M. Saldanha, M. Correa, G. Correa, D. Palomino, M. Porto, B. Zatt, and L. Agostini, "An overview of dedicated hardware designs for state-of-the-art AV1 and h.266/VVC video codecs," in *Proc. IEEE International Conference on Electronics, Circuits and Systems (ICECS)*. IEEE, Nov. 2020.
- [16] C. Herglotz and A. Kaup, "Video decoding energy estimation using processor events," in *Proc. IEEE International Conference on Image Processing (ICIP)*, Beijing, China, Sep. 2017.
- [17] T. Mallikarachchi, D. S. Talagala, H. K. Arachchi, and A. Fernando, "A feature based complexity model for decoder complexity optimized HEVC video encoding," in *Proc. IEEE International Conference on Consumer Electronics (ICCE)*, Las Vegas, NV, USA, Jan. 2017.
- [18] C. Herglotz, D. Springer, M. Reichenbach, B. Stabernack, and A. Kaup, "Modeling the energy consumption of the HEVC decoding process," *IEEE Transactions on Circuits and Systems for Video Technology*, vol. 28, no. 1, pp. 217–229, Jan. 2018.
- [19] M. Kränzler, C. Herglotz, and A. Kaup, "Extending video decoding energy models for 360° and HDR video formats in HEVC," in *Proc. Picture Coding Symposium (PCS)*, Ningbo, China, Nov. 2019.
- [20] —, "Decoding energy modeling for versatile video coding," in *Proc. International Conference on Image Processing (ICIP)*, Abu Dhabi, United Arab Emirates, Oct. 2020.
- [21] C. Herglotz and A. Kaup, "Decoding energy estimation of an HEVC hardware decoder," in *2018 IEEE International Symposium on Circuits and Systems (ISCAS)*, Florence, Italy, May 2018.
- [22] C. Herglotz, S. Coulombe, C. Vazquez, A. Vakili, A. Kaup, and J.-C. Grenier, "Power modeling for video streaming applications on mobile devices," *IEEE Access*, vol. 8, pp. 70 234–70 244, Apr. 2020.
- [23] M. Kränzler, A. Kaup, and C. Herglotz, "Estimating software and hardware video decoder energy using software decoder profiling," in *Proc. 36th SBC/SBMicro/IEEE/ACM Symposium on Integrated Circuits and Systems Design (SBCCI)*, Rio de Janeiro, Brazil, Aug. 2023.
- [24] C. Herglotz, A. Heindel, and A. Kaup, "Decoding-energy-rate-distortion optimization for video coding," *IEEE Transactions on Circuits and Systems for Video Technology*, vol. 29, no. 1, pp. 171–182, Jan. 2019.
- [25] M. Kränzler, C. Herglotz, and A. Kaup, "Energy Efficient Video Decoding for VVC Using a Greedy Strategy Based Design Space Exploration," *IEEE Transactions on Circuits and Systems for Video Technology*, vol. 32, no. 7, pp. 4696–4709, Jul. 2022.
- [26] M. Kränzler, A. Wieckowski, G. Ramasubbu, B. Bross, A. Kaup, D. Marpe, and C. Herglotz, "Optimized decoding-energy-aware encoding in practical VVC implementations," in *Proc. International Conference on Image Processing (ICIP)*, Bordeaux, France, Oct. 2022.
- [27] M. Kränzler, A. Kaup, and C. Herglotz, "Advanced design space exploration for joint energy and quality optimization for VVC," in *Proc. Picture Coding Symposium (PCS)*, San Jose, CA, USA, Dec. 2022.
- [28] A. Tissier, A. Mercat, T. Amestoy, W. Hamidouche, J. Vanne, and D. Menard, "Complexity reduction opportunities in the future VVC intra encoder," in *Proc. International Workshop on Multimedia Signal Processing (MMSp)*, Kuala Lumpur, Malaysia, Sep. 2019.

- [29] H. Amirpour, V. V. Menon, S. Afzal, R. Prodan, and C. Timmerer, "Optimizing video streaming for sustainability and quality: The role of preset selection in per-title encoding," in *Proc. International Conference on Multimedia and Expo (ICME)*, Brisbane, Australia, Jul. 2023.
- [30] Videolan. x264 Encoder. Accessed 2021-09. [Online]. Available: <https://code.videolan.org/videolan/x264.git>
- [31] HHI Fraunhofer. JM Decoder. Accessed 2021-09. [Online]. Available: <https://vcgit.hhi.fraunhofer.de/jvet/JM>
- [32] Fast Forwards MPEG (FFmpeg). Accessed 2018-11-14. [Online]. Available: <http://ffmpeg.org/>
- [33] Videolan. x265 Encoder. Accessed 2021-09. [Online]. Available: <http://hg.videolan.org/x265>
- [34] HHI Fraunhofer. HM Decoder. Accessed 2021-09. [Online]. Available: <https://vcgit.hhi.fraunhofer.de/jvet/HM>
- [35] openHEVC. Accessed 2021-02-25. [Online]. Available: <https://github.com/OpenHEVC/openHEVC>
- [36] Fraunhofer HHI VVenC Software Repository. Accessed: Jan 2022. [Online]. Available: <https://github.com/fraunhoferhhi/vvenc>
- [37] Joint Video Exploration Team (JVET). VVC test model reference software. [Online]. Available: https://vcgit.hhi.fraunhofer.de/jvet/VVCSoftware_VTM/
- [38] Fraunhofer HHI VVdeC Software Repository. Accessed: Jan 2022. [Online]. Available: <https://github.com/fraunhoferhhi/vvdec>
- [39] Google. libvpx Codec. Accessed 2021-10. [Online]. Available: <https://chromium.googlesource.com/webm/libvpx/>
- [40] A. for Open Media. libaom Codec. Accessed 2022-03. [Online]. Available: <https://aomedia.googlesource.com/aom/>
- [41] DAV1D. DAV1D Software. Accessed 2022-03. [Online]. Available: <https://code.videolan.org/videolan/dav1d>
- [42] Google. AVM Codec. Accessed 2022-07. [Online]. Available: <https://gitlab.com/AOMediaCodec/avm>
- [43] T. Wiegand, G. Sullivan, G. Bjontegaard, and A. Luthra, "Overview of the h.264/AVC video coding standard," *IEEE Transactions on Circuits and Systems for Video Technology*, vol. 13, no. 7, pp. 560–576, Jul. 2003.
- [44] G. J. Sullivan, J.-R. Ohm, W.-J. Han, and T. Wiegand, "Overview of the high efficiency video coding (HEVC) standard," *IEEE Transactions on Circuits and Systems for Video Technology*, vol. 22, no. 12, pp. 1649–1668, Dec. 2012.
- [45] B. Bross, Y.-K. Wang, Y. Ye, S. Liu, J. Chen, G. J. Sullivan, and J.-R. Ohm, "Overview of the Versatile Video Coding (VVC) standard and its applications," *IEEE Transactions on Circuits and Systems for Video Technology*, vol. 31, no. 10, pp. 3736–3764, Oct. 2021.
- [46] A. Wieckowski, J. Brandenburg, T. Hinz, C. Bartnik, V. George, G. Hege, C. Helmrich, A. Henkel, C. Lehmann, C. Stoffers, I. Zupancic, B. Bross, and D. Marpe, "VVenC: An open and optimized VVC encoder implementation," in *Proc. IEEE International Conference on Multimedia Expo Workshops (ICMEW)*, pp. 1–2.
- [47] A. Wieckowski, G. Hege, C. Bartnik, C. Lehmann, C. Stoffers, B. Bross, and D. Marpe, "Towards a live software decoder implementation for the upcoming Versatile Video Coding (VVC) codec," in *Proc. IEEE International Conference on Image Processing (ICIP)*, pp. 3124–3128.
- [48] D. Mukherjee, J. Bankoski, A. Grange, J. Han, J. Koleszar, P. Wilkins, Y. Xu, and R. Bultje, "The latest open-source video codec VP9 - an overview and preliminary results," in *2013 Picture Coding Symposium (PCS)*, Dec. 2013.
- [49] Y. Chen, D. Mukherjee, J. Han, A. Grange, Y. Xu, S. Parker, C. Chen, H. Su, U. Joshi, C.-H. Chiang, Y. Wang, P. Wilkins, J. Bankoski, L. Trudeau, N. Egge, J.-M. Valin, T. Davies, S. Midtskogen, A. Norkin, P. de Rivaz, and Z. Liu, "An overview of coding tools in AV1: the first video codec from the alliance for open media," *APSIPA Transactions on Signal and Information Processing*, vol. 9, 2020.
- [50] X. Zhao, Z. Lei, A. Norkin, T. Daede, and A. Tourapis, "AV2 common test conditions v1.0," document, CWG-B005o v1, Jan. 2021.
- [51] H. David, E. Gorbato, U. R. Hanebutte, R. Khanna, and C. Le, "RAPL: Memory power estimation and capping," in *Proc. ACM/IEEE International Symposium on Low-Power Electronics and Design (ISLPED)*, Austin, TX, USA, Aug. 2010.
- [52] A. Katsenou, X. Wang, D. Schien, and D. Bull, "Comparative study of hardware and software power measurements in video compression," in *Proc. Picture Coding Symposium (PCS)*, Taichung, Taiwan, June 2024.
- [53] Radxa. Rock 5B Hardware Details. Accessed 2023-11. [Online]. Available: <https://wiki.radxa.com/Rock5/hardware/5b>
- [54] A. J. Izenman, *Modern Multivariate Statistical Techniques: Regression, Classification, and Manifold Learning*. Springer, 2013.
- [55] T. F. Coleman and Y. Li, "An interior trust region approach for nonlinear minimization subject to bounds," *SIAM Journal on optimization*, vol. 6, no. 2, pp. 418–445, May 1996.
- [56] C. E. Rasmussen and C. K. I. Williams, *Gaussian Processes for Machine Learning*. Cambridge, MA, USA: MIT Press, 2006.
- [57] Matlab. Gaussian process regression models. Accessed 2023-11. [Online]. Available: <https://de.mathworks.com/help/stats/gaussian-process-regression-models.html>
- [58] T. Hastie, R. Tibshirani, and J. Friedman, *The Elements of Statistical Learning: Data Mining, Inference, and Prediction, Second Edition*. Springer New York, NY, USA, 2009.
- [59] P. A. Watters and S. Boslaugh, *Statistics in a nutshell: A desktop quick reference*. Sebastopol, CA, USA: O'Reilly, 2008.
- [60] J. Lee Rodgers and W. A. Nicewander, "Thirteen ways to look at the correlation coefficient," *The American Statistician*, vol. 42, no. 1, pp. 59–66.